
TRANSITION FROM LAMINAR TO TURBULENT PIPE FLOW AS A PROCESS OF GROWING MATERIAL INSTABILITIES

A PREPRINT

 **Saptarshi Kumar Lahiri***

Faculty of Civil and Environmental Engineering
Technion Israel Institute of Technology
Haifa, IL - 3200003
saptarshi@campus.technion.ac.il

 **Konstantin Volokh**

Faculty of Civil and Environmental Engineering
Technion Israel Institute of Technology
Haifa, IL - 3200003
cvolokh@technion.ac.il

May 13, 2024

ABSTRACT

In this work, we simulate the transition to turbulence in the pipe flow based on the modified NS theory incorporating the viscous fluid strength in the constitutive equations. The latter concept enriches theory by allowing for material instabilities in addition to the kinematic ones. We present results of comparative numerical simulations based on the classical NS model and the NS model enhanced with the finite viscous strength. As expected, simulations based on the classical NS model exhibit stable laminar flow in contrast to experimental observations. Conversely, simulations based on the modified NS model with viscous strength exhibit instabilities and transition to turbulence per experimental observations. The transition to turbulence is triggered by the growing material instabilities.

Keywords Transition into turbulence · viscous strength model · pipe flow simulation · Navier-Stokes model

1 Introduction

Considering pipe flow, Osborne Reynolds [1883, 1895] introduced a non-dimensional parameter $Re = \rho v D / \eta$, in which ρ is the mass density of the fluid, v is the mean velocity, D is the diameter of the pipe, and η is the viscosity of the fluid. Reynolds assumed that the transition from laminar to turbulent flow occurred at some critical number Re_{cr} . Experimental estimates of this critical number for water vary from 1700 and 2300 Faisst and Eckhardt [2004], Eckhardt [2007] to 3000 Eckhardt [2009]. Recently, Avila et al. [2011] experimentally studied laminar flow through a 15 m long pipe with a diameter of 4 mm and observed that at $Re_{cr} \approx 2400$ the laminar flow became unstable and indicated transition to turbulence.

Theoretical explanations of the transition to turbulence have a long history Tanner and Walters [1998], Manneville [2015, 2016], Barkley [2016], Eckert [2019, 2022], Feigenbaum [1978], Gollub and Swinney [1975] and debates proceed nowadays. Unfortunately, the linear instability analysis cannot capture the onset of failure of the laminar flow, which is observed in experiments. The linear instability analysis tracks the evolution of infinitesimal or small perturbations, e.g., molecular fluctuations, which always exist. Such perturbations do not develop into transitional flow according to the Navier-Stokes theory Romanov [1973], Landau and Lifshitz [2013].

To accommodate the experimentally observed transition to turbulence within the framework of the Navier-Stokes theory, some authors assume the existence of finite or large perturbations in the laminar flow Peixinho and Mullin [2006], Eckhardt [2007, 2009]. The physical grounds for such an assumption are disputable. Interestingly, Wgnanski and Champagne Wgnanski and Champagne [1973] observed that the enforcement of the finite perturbations did not always ensure instability.

We note in passing that the conventional NS approach also struggles to explain the physical mechanism of the drag reduction when a small amount of polymer molecules is added to a Newtonian solvent as reported widely in the

*Alternate mail - lahiriaayan22@gmail.com— Funded by Israel Science Foundation

literature Toms [1949], Boelens and Muthukumar [2016], Bewersdorff [1995], Nadolink and Haigh [1995], Ptasinski et al. [2003], Xi and Bai [2016], Lumley [1969].

The difficulty of the classical NS theory to explain some of the experimentally observed transitions to turbulence led Volokh Volokh [2009, 2013, 2018] to assume that considerations of purely kinematic instabilities of the laminar flow were not enough and material instabilities of the flow should be taken into account as well. The latter extension of the NS theory can be done, for example, by the enforcement of finite viscous strength in the constitutive law. Physically, it means that viscosity drops at the critical strain rate because internal friction breaks down leading to instability of the laminar flow. The viscous stress corresponding to the critical strain rate is termed the viscous strength of the fluid. It is a material property.

Quite amazingly, the recent molecular dynamic simulations by Raghavan and Ostoja-Starzewski Raghavan and Ostoja-Starzewski [2017] confirm the assumption of viscous strength in the continuum mechanics formulation.

Despite its theoretical promise and some analytical results Volokh [2009, 2013, 2018], the proposed modified NS constitutive model with viscous strength was not examined in specific numerical simulations of a three-dimensional pipe flow. This gap is filled in the present work. Results of numerical simulations are reported below, which show the transition to turbulence in the pipe flow. This transition is due to the process of growing material instabilities.

2 Navier-Stokes model enhanced with viscous strength

In this section, we summarize the governing equations. They include the linear momentum balance in the standard form

$$\rho \frac{\partial \mathbf{v}}{\partial t} + \rho(\text{grad} \mathbf{v}) \cdot \mathbf{v} = -\text{grad} p + \text{div} \boldsymbol{\tau}, \quad (1)$$

where ρ is the mass density; \mathbf{v} is the velocity obeying the incompressibility condition $\text{div} \mathbf{v} = 0$; t is time; p is the hydrostatic pressure; and $\boldsymbol{\tau}$ is the viscous stress tensor.

The governing equations also include the constitutive law. For Newtonian fluids, the viscous stress is proportional to the strain rate

$$\boldsymbol{\tau} = 2\eta \mathbf{D}, \quad (2)$$

where η is the fluid viscosity and $\mathbf{D} = (\text{grad} \mathbf{v} + \text{grad} \mathbf{v}^T) / 2$ is the strain rate tensor equal to the symmetric part of the velocity gradient.

In the viscous strength model Volokh [2009], a finite strain rate limiter is incorporated in the viscosity function that remains constant until a critical point, beyond which the viscosity drops to zero representing a breakdown of contacts between fluid layers

$$\eta^* = \eta \exp \left[- \left(\frac{\mathbf{D} : \mathbf{D}}{\phi^2} \right)^m \right], \quad (3)$$

where $\mathbf{D} : \mathbf{D} = \text{tr} [\mathbf{D} \mathbf{D}^T]$ is the squared equivalent scalar strain rate; m is a constant; and ϕ is the critical equivalent strain rate, which is a saturation limit for the material stability of the fluid.

The viscosity function has essentially two modes – nonzero constant, which describes a classical Newtonian fluid, and zero constant, corresponding to the ideal fluid with negligible internal friction:

$$\eta^* = \begin{cases} \eta & \text{when } \mathbf{D} : \mathbf{D} < \phi^2 \\ 0 & \text{when } \mathbf{D} : \mathbf{D} > \phi^2, \end{cases} \quad (4)$$

By increasing the magnitude of constant m in Eq. 3, it is possible to approach the step function that physically means a breakdown in the internal friction between fluid layers – Fig. 1a.

Accordingly, the modified constitutive model incorporating the viscous strength becomes

$$\boldsymbol{\tau} = 2\eta^* \mathbf{D}. \quad (5)$$

For the sake of clarification, let us consider shear flow with nonzero strain rate component D_{xy} and stress τ_{xy} . In this case, the constitutive law takes the form

$$\frac{\tau_{xy}}{\eta\phi} = 2 \left(\frac{D_{xy}}{\phi} \right) \exp \left[-2^m \left(\frac{D_{xy}}{\phi} \right)^{2m} \right]. \quad (6)$$

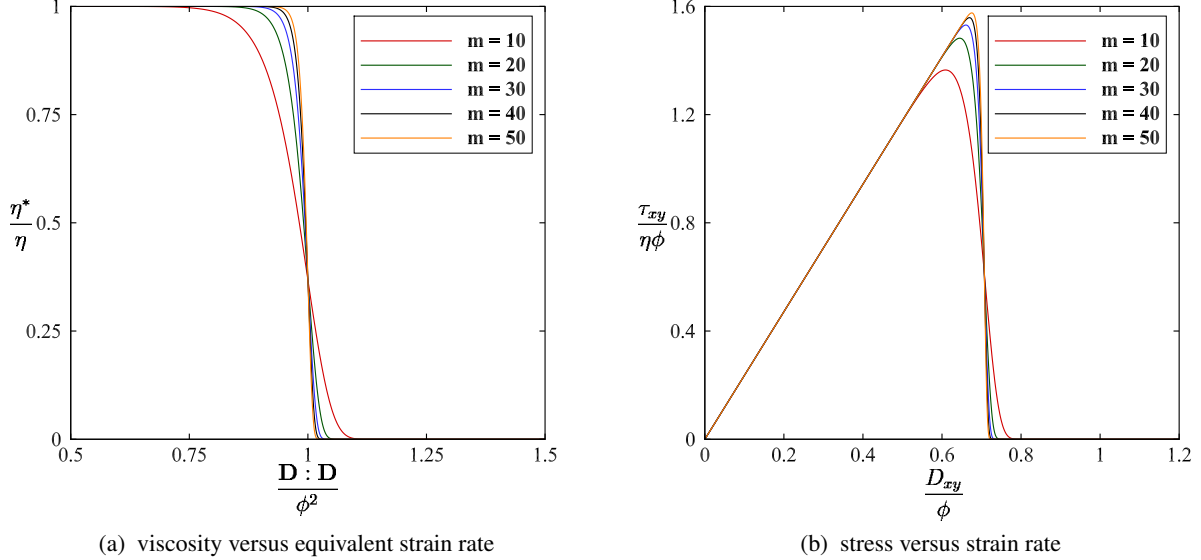


Figure 1: Viscous strength model

Its graphical representation in Fig. 1b shows that, unlike the classical NS theory, the shear stress possesses a finite limit – strength – indicating the breakdown of internal viscous friction. The strain rate corresponding to this stress bound can be obtained by solving $d\tau_{xy}/dD_{xy} = 0$ for Eq. 6, which results in

$$\frac{D_{xy}}{\phi} = \left[\frac{1}{2^{m+1} m} \right]^{\frac{1}{2m}}. \quad (7)$$

Hence, the viscous strength of the fluid becomes $\tau_{xy} = \sqrt{2}\eta\phi$ for $m \gg 1$.

Remark 1 We note that the conventional Navier-Stokes assumption of the perfectly intact viscous bonds is an extreme case of the viscous strength model with $\phi \rightarrow \infty$. In other words, the traditional NS model possesses infinitely large viscous strength. The latter means that the friction between adjacent fluid layers is always ideal and the viscous stress can increase infinitely with the increasing strain rate. Such property of the NS model is doubtful on physical grounds because no unbreakable materials really exist.

Remark 2 The model parameter m helps in the mathematical smoothing of the step function. For materials with finite viscous stress, the critical strain rate can be obtained with the help of equality $\lim_{m \rightarrow \infty} \left[\frac{1}{2^{m+1} m} \right]^{\frac{1}{2m}} = \frac{1}{\sqrt{2}}$.

3 Pipe flow simulations

In this section, we describe simulations of a three-dimensional pipe flow through a 60 mm long perfectly straight cylindrical pipe with a uniform circular cross-section of diameter $D = 4$ mm – see Fig. 2a. We use two material models:

- (a) Conventional Navier-Stokes model with infinite viscous strength, further abbreviated CV;
- (b) Modified Navier-Stokes model with finite viscous strength, further abbreviated VSM.

The fluid is water with mass density $\rho = 1000$ kg/m³, viscosity $\eta = 0.001$ kg/m/s, critical equivalent strain rate Volokh [2009, 2013] $\phi = 848.5$ s⁻¹, and constant $m = 20$. For the sake of comparison, specific sections are chosen in the pipe (see Fig. 2b) to record measurements of respective simulations.

We utilize commercial software ANSYS-2021R2 in computations. The spatial unstructured mesh has 1,476,706 elements with 1,514,133 nodes. The discretization at a typical cross-section of the pipe is shown in Fig. 3. The wall of the pipe is stationary with no-slip boundary conditions. It is further assumed that the fluid flow is initially stable and, hence, a fully developed parabolic flow profile (Fig. 4) is provided at the inlet, and zero-pressure boundary conditions are incorporated at the outlet of the pipe.

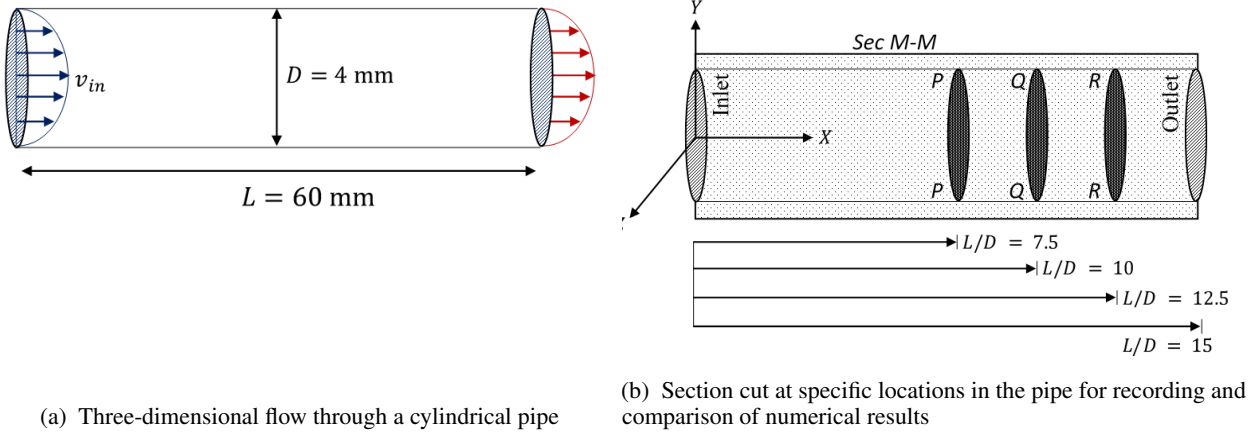


Figure 2: Schematic diagram of the problem

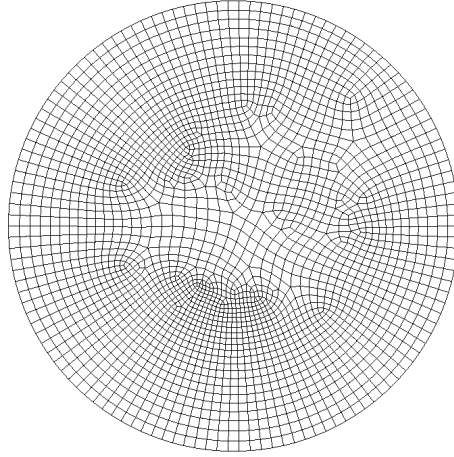


Figure 3: Typical cross-sectional mesh

Simulations are performed for different load cases by varying the peak inlet velocity v_{in} . By specifying the inlet velocity, it is easy to have a perception of the velocity gradient generated within the flow. An approximate measure of the Reynolds number can be assessed based on a constant velocity \hat{v} that would generate the stable fully developed velocity profile at the inlet face as shown in Fig. 4. The relationship between \hat{v} and v_{in} can be obtained from the laminar flow theory as $\hat{v} = 2v_{in}/3$. Hence, the Reynolds number becomes $Re = 2\rho v_{in}D/(3\eta)$. Table 1 lists the inlet velocities and corresponding Reynolds numbers for all loading cases considered in numerical examples.

The choice of an appropriate numerical framework is essential to capture the underlying physical processes governing the genesis of material instability in a pipe flow problem. For realistic 3D flows, the direct numerical solution becomes intractable. Instead, the large Eddy simulation (LES) is routinely used to save time. The specific advantage of LES lies in effectively reducing computational costs, yet capturing the transition to turbulence with reasonable accuracy.

Table 1: Inlet velocity (v_{in}) and Reynolds number (Re) for different load cases ($\rho = 1000 \text{ kg/m}^3$; $D = 4 \text{ mm}$; $\eta = 0.001 \text{ kg/m/s}$)

| Load case | Inlet velocity (v_{in}) (m/s) | $Re = \frac{2\rho v_{in}D}{3\eta}$ |
|-----------|-----------------------------------|------------------------------------|
| A | 0.6 | 1600 |
| B | 0.7 | 1867 |
| C | 0.9 | 2400 |

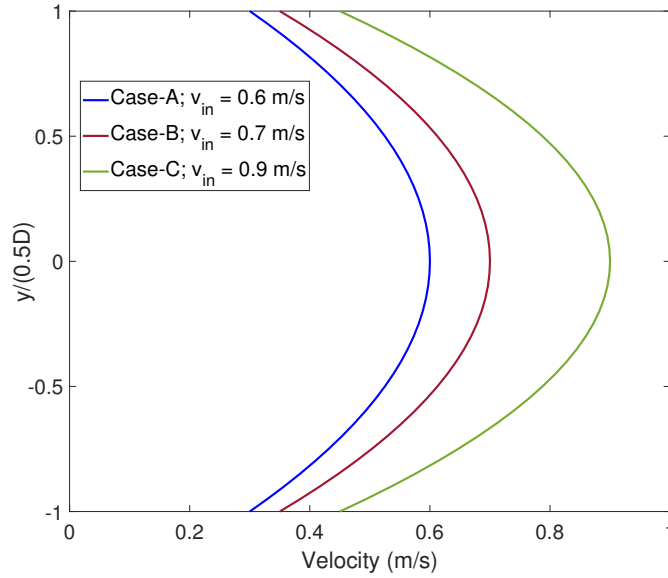


Figure 4: Velocity profiles provided at the inlet of the pipe for different simulation cases

The LES filters out the small-scale eddies, insignificant to turbulence, from the solution and determines the unknowns by a sub-grid turbulence model. Among various sub-grid turbulence models Smagorinsky [1963], Germano et al. [1991], Nicoud and Ducros [1999], Lilly [1992], Shur et al. [2008] reported in the literature, the wall adopted local eddy-viscosity (WALE) Nicoud and Ducros [1999] approach is advantageous for problems related to transitional flows. In principle, the WALE model represents proper scaling at the wall functions and returns a zero turbulent eddy viscosity (μ_t) for laminar shear flows, which makes it appropriate to treat laminar zones in the fluid domain.

In the first set of simulations, with the peak inlet velocity of $v_{in} = 0.6$ m/s i.e. $Re \approx 1600$ (refer to Table 1) the CV model (i.e. the classical NS model with infinite viscous strength) predicts a stable laminar flow; whereas in the VSM (i.e. the modified NS model with finite viscous strength) we can observe instability in the flow. This highly localized material instability triggers deviation from laminar flow near the outlet of the pipe (Fig. 5a). The onset of the instability is visible in the profile of the longitudinal velocity across the cross section of the pipe at a distance $L/D = 10$ from the inlet face (section Q-Q in Fig. 2b) of the pipe (Fig. 5b).

As we increase the inlet velocity to $v_{in} = 0.7$ m/s i.e., $Re \approx 1867$, the CV model still predicts a perfectly stable solution and the flow remains perfectly laminar. However, in the VSM solution we can observe a visible deviation from the laminar flow pattern (Fig. 5c). In this case, the instabilities are more pronounced than the first case. The contour of longitudinal velocity across the cross-section of the pipe at a distance $L = 10D$ (section Q-Q in Fig. 2b) in Fig. 5d demonstrates a clear transition to turbulence.

With the further increase in the inlet velocity to $v_{in} = 0.9$ m/s, that is, $Re \approx 2400$, the VSM simulation produces a turbulent flow with eddies spread globally along the length of the pipe (Fig. 5e) while the CV model still provides a stable laminar flow. Like in the previous examples, in section Q-Q, $L = 10D$ distant from the inlet, Fig. 5f indicates complete loss of the laminar mode in the longitudinal flow.

Instabilities in the flow generates localised puffs or fluctuations in the transverse velocity profile in the channel. The VSM simulation reports that the peak fluctuation is ≈ 0.1 m/s, whereas for the CV model we do not notice any significant fluctuation for $v_{in}=0.6$ m/s (Figs. 6a-6b). These fluctuations are highly localized in nature and the flow remains laminar. As we increase the inlet velocity to $v_{in}=0.7$ m/s the localised puffs magnify and the peak magnitude reaches ≈ 0.16 m/s (Figs. 7a-7b). For $v_{in} = 0.9$ m/s, that is, $Re \approx 2400$, the VSM simulation yields a turbulent flow with eddies with a maximum variation in the transverse velocity of ≈ 0.25 m/s (refer to Figs. 8a-8b).

Remark 3 We note that the standard viscometer/rheometer tests are useless for the calibration of the fluid strength. Indeed, to observe the drop of viscosity, all fluid particles should reach the critical state simultaneously. That is practically impossible and the viscosity drops randomly at some points where the local material instability develops. Thus, only the observation of the onset of transition to chaos is suitable for calibration of the fluid strength. This issue is

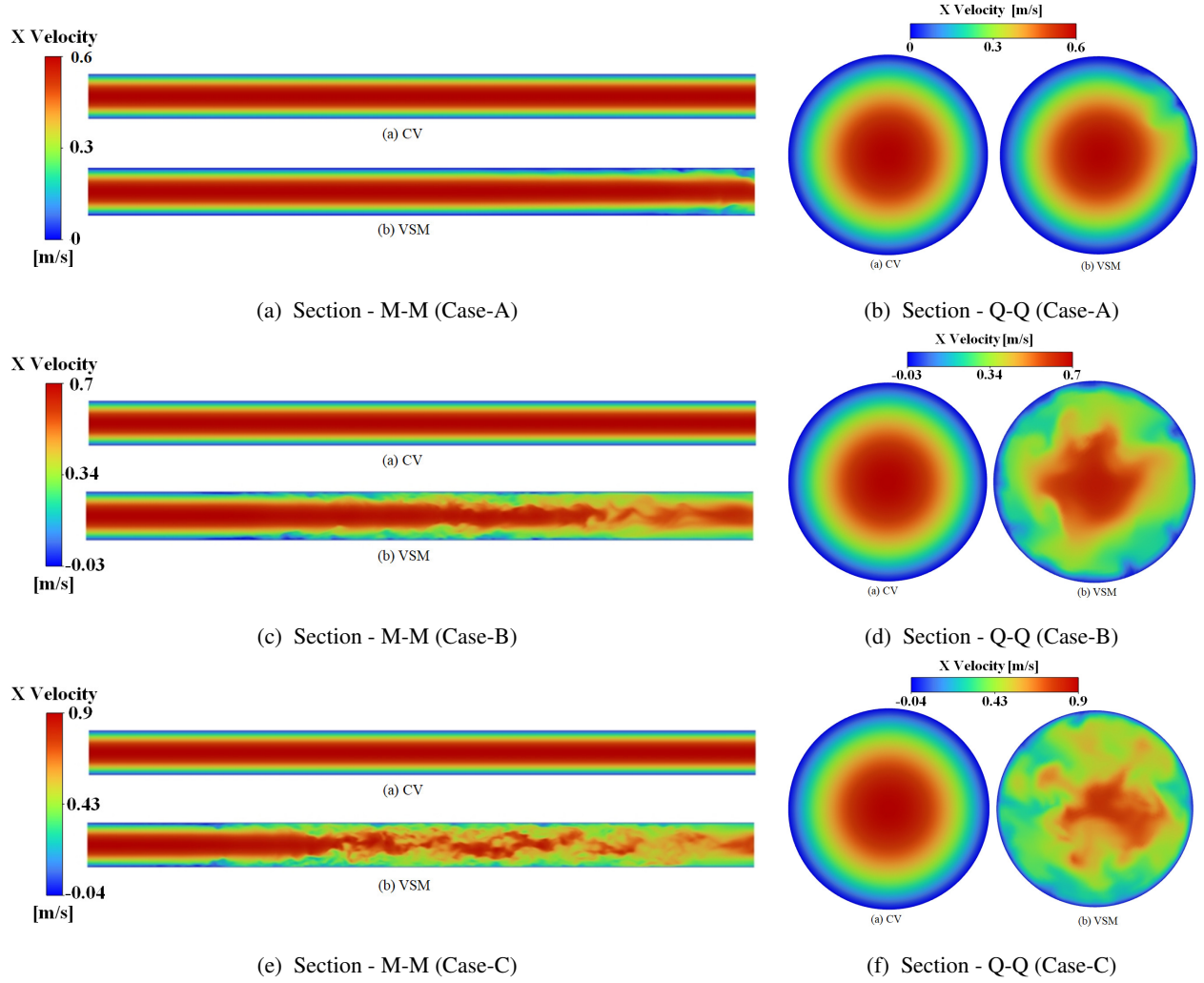


Figure 5: Variation of flow velocity (v_x) (refer to sections M-M, and Q-Q in Fig.2b) for different inlet velocity conditions — A, B, & C (Table 1)

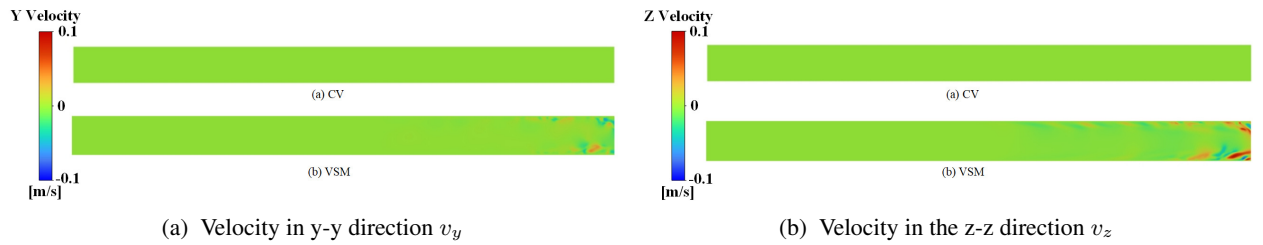


Figure 6: Variation of transverse velocity along the length of the pipe at section M-M (refer to Fig.2b) for inlet velocity case A ; $v_{in}=0.6m/s$

discussed with great attention in Volokh [2013], to which the reader is referred.

Remark 4 We again emphasize that we used the same techniques of large eddy simulations for both the classical Navier-Stokes model and the model enhanced with strength. The latter model presents viscosity as a step function with non-zero and zero viscosity coefficients. The theory of large-eddy simulations is equally applicable to both constitutive models and the comparison of the results is objective.

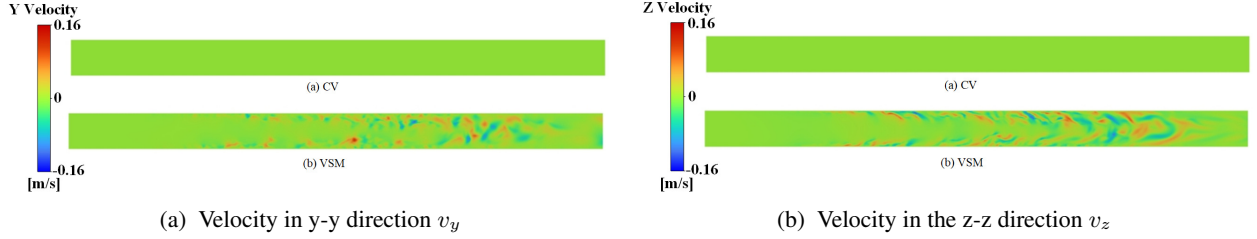


Figure 7: Variation of transverse velocity along the length of the pipe at section M-M (refer to Fig.2b) for inlet velocity case B ; $v_{in}=0.7m/s$

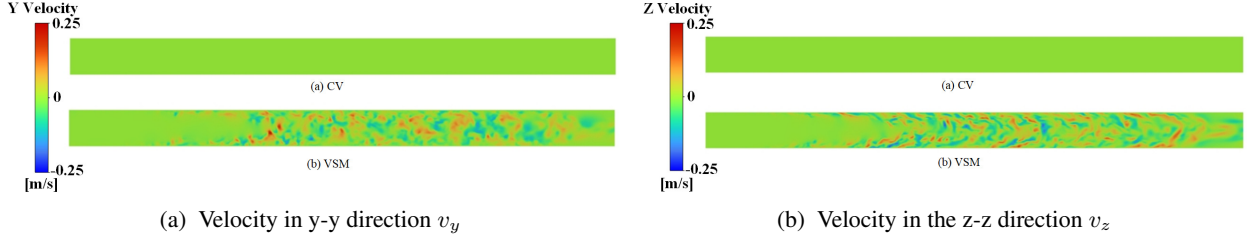


Figure 8: Variation of transverse velocity along the length of the pipe at section M-M (refer to Fig.2b) for inlet velocity case C ; $v_{in}=0.9m/s$

4 Discussion

Based on the numerical simulations reported above, we suggest that the turbulence is the result of two main events: the genesis of material instabilities in the laminar flow and the transition and growth of local instabilities into large eddies. Instabilities appear initially due to the reduction in viscous stresses with the increase in flow strain rates.

Table 2: Maximum strain rate and wall shear stress in the channel section for the CV model or conventional Navier-Stokes equation under different inlet velocity conditions ($\phi = 848.5 \text{ s}^{-1}$)

| Case | Inlet velocity | Max strain rate | Max wall shear | $\frac{\sqrt{\mathbf{D} : \mathbf{D}}}{\phi}$ |
|------|-------------------|---|----------------------|---|
| | (v_{in}) m/s | $(\sqrt{\mathbf{D} : \mathbf{D}})$ s^{-1} | (τ_{max}) Pa | |
| A | 0.6 | 596.7 | 0.60 | 0.70 |
| B | 0.7 | 696.2 | 0.71 | 0.82 |
| C | 0.9 | 895.2 | 0.91 | 1.06 |

Our simulations and some parameters collected in Table 2 prompt that material instabilities are born at $v_{in} = 0.6 \text{ m/s}$. The latter means that shear stresses begin to drop near the pipe wall, small eddies appear and start to grow, and the flow deviates from the laminar (Fig. 9a; Case-A) behavior. When the flow velocity increases to $v_{in} = 0.7 \text{ m/s}$, the fluid remains within the transition range, but the instabilities and eddies expand over a wider zone (Fig. 9a; Case-B). By increasing the inlet velocity to $v_{in} = 0.9 \text{ m/s}$ (Case-C), the eddies become large and spread throughout the pipe (Fig. 9a; Case-C).

Once the instability arises, the drop in the shear stress near the zone of instability induces disturbances in transverse velocities. The magnitude of the disturbances increases with increasing flow velocity (Figs. 9b-9c). The turbulence moves towards the inlet face of the pipe with an increase in the inlet velocity of the fluid. The variation in axial velocity in section M-M is marginal for $v_{in} = 0.6 \text{ m/s}$.

Fig. 10 presents another interesting phenomenon: as the fluid loses its stability, the strain rates are magnified near the zone of instability. Subsequently, during the transition to turbulence, the magnified strain rates start propagating towards the center of the pipe.

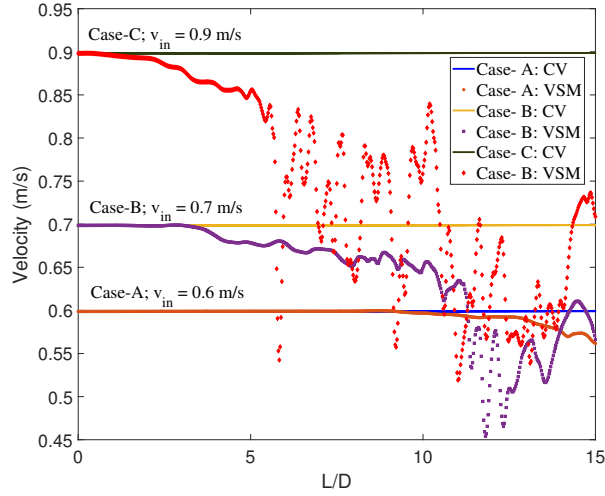
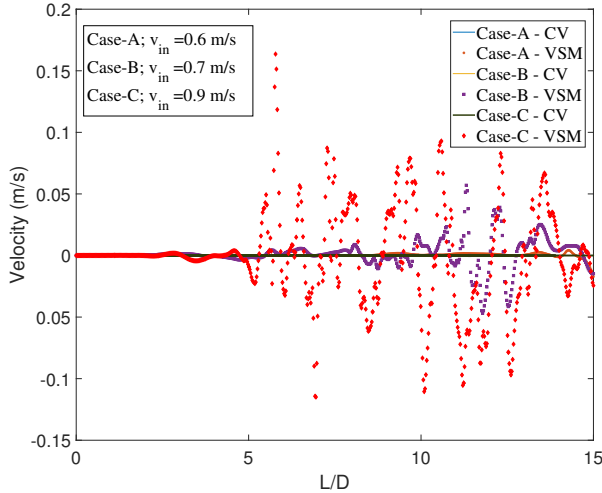
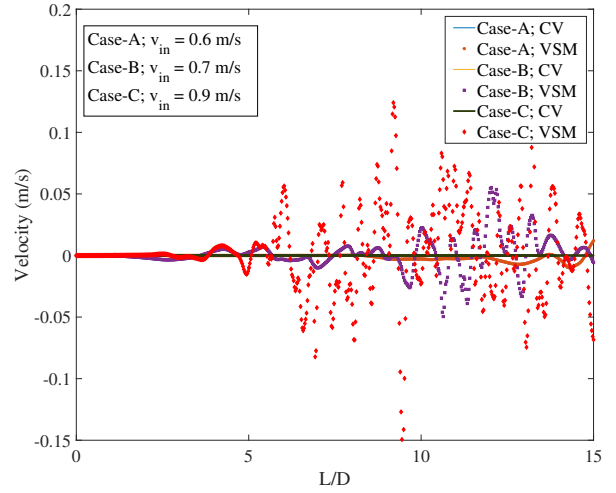
(a) Profile of longitudinal velocity v_x (b) Profile of transverse velocity v_y (c) Profile of transverse velocity v_z

Figure 9: Variation in flow velocities along the direction of pipe flow at section M-M (cut at the midplane where $z = 0$, refer to Fig. 2b) for velocity cases A, B, and C

The flow profiles generated in the simulations demonstrate the ability of the constitutive model to capture the developing turbulence. The initial visible sign of instability originates in Case-A at a distance of $L = 10D$ from the inlet face of the pipe (Fig. 11a). As the inlet velocity increases to 0.7 m/s and 0.9 m/s in Case-B and Case-C respectively, the local instability diffuses towards the inlet face resulting in turbulence much closer to the inlet (Figs. 11b-11c). While in Fig. 11a the flow remains laminar up to $L = 12.5D$ from the inlet, the laminar zone is predominantly restricted up to $L = 7.5D$ in Fig. 11b. A further increase in the inlet velocity makes the flow turbulent even before $L = 7.5D$ - Fig. 11c.

5 Conclusion

In this work, we presented results of numerical simulations of pipe flow based on Navier-Stokes theory with and without viscous strength. These results show that viscous strength is crucial for the appearance of material instabilities of the flow and is consistent with the experimental observation of Avila et al. [2011]. Such material instabilities trigger local transitions to a chaotic flow that develops into turbulence. We hypothesize that material instabilities compete with the kinematic ones in the process of the transition to turbulence. Unfortunately, the classical

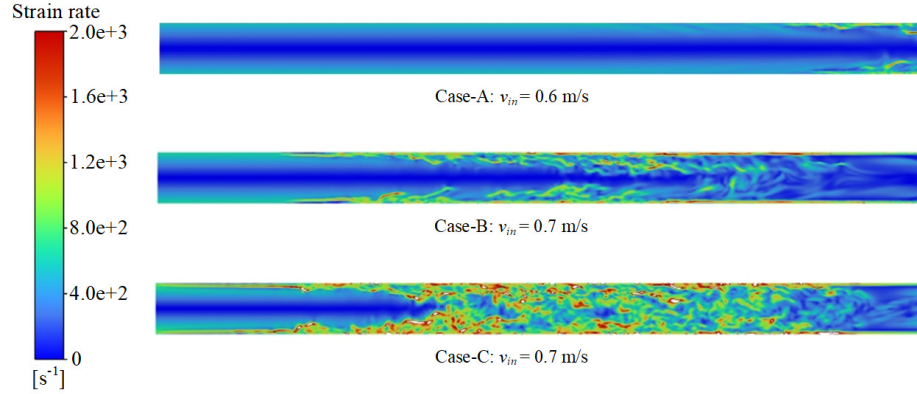


Figure 10: Magnification of the strain rate ($\sqrt{\mathbf{D} : \mathbf{D}}$) in the M-M section (at $z = 0$, in Fig. 2b) for different inlet velocity conditions — Case – A,B, & C

Navier-Stokes model cannot capture the material instabilities and, thus, cannot describe the transition to turbulence in kinematically stable flows. Enhancement of the classical model with finite viscous strength opens new ways to simulate and understand the transition to turbulence.

Acknowledgements

This work was supported by the Israel Science Foundation (ISF-394/20).

Author contributions statement

K.V. conceived the idea, S.K.L. conducted the numerical simulations, and S.K.L. and K.V. analysed the results. All authors reviewed the manuscript.

Data Availability Statement

The data sets used and analysed during the current study are available from the corresponding author on reasonable request.

References

- O. Reynolds. An experimental investigation of the circumstances which determine whether the motion of water shall be direct or sinuous, and of the law of resistance in parallel channels. *Philosophical Transactions of the Royal Society London*, (174):935–982, 1883.
- Osborne Reynolds. On the dynamical theory of incompressible viscous fluids and the determination of the criterion. *Philosophical Transactions of the Royal Society London*, (186):123–164, 1895.
- Holger Faisst and Bruno Eckhardt. Sensitive dependence on initial conditions in transition to turbulence in pipe flow. *Journal of Fluid Mechanics*, 504:343–352, 2004.
- Bruno Eckhardt. Turbulence transition in pipe flow: some open questions. *Nonlinearity*, 21(1):T1, 2007.
- Bruno Eckhardt. Introduction. turbulence transition in pipe flow: 125th anniversary of the publication of reynolds’ paper. *Philosophical Transactions of the Royal Society A: Mathematical, Physical and Engineering Sciences*, 367 (1888):449–455, 2009.
- Kerstin Avila, David Moxey, Alberto De Lozar, Marc Avila, Dwight Barkley, and Björn Hof. The onset of turbulence in pipe flow. *Science*, 333(6039):192–196, 2011.
- Roger I Tanner and Kenneth Walters. *Rheology: An Historical Perspective*. Elsevier, 1998.
- Paul Manneville. On the transition to turbulence of wall-bounded flows in general, and plane couette flow in particular. *European Journal of Mechanics-B/Fluids*, 49:345–362, 2015.

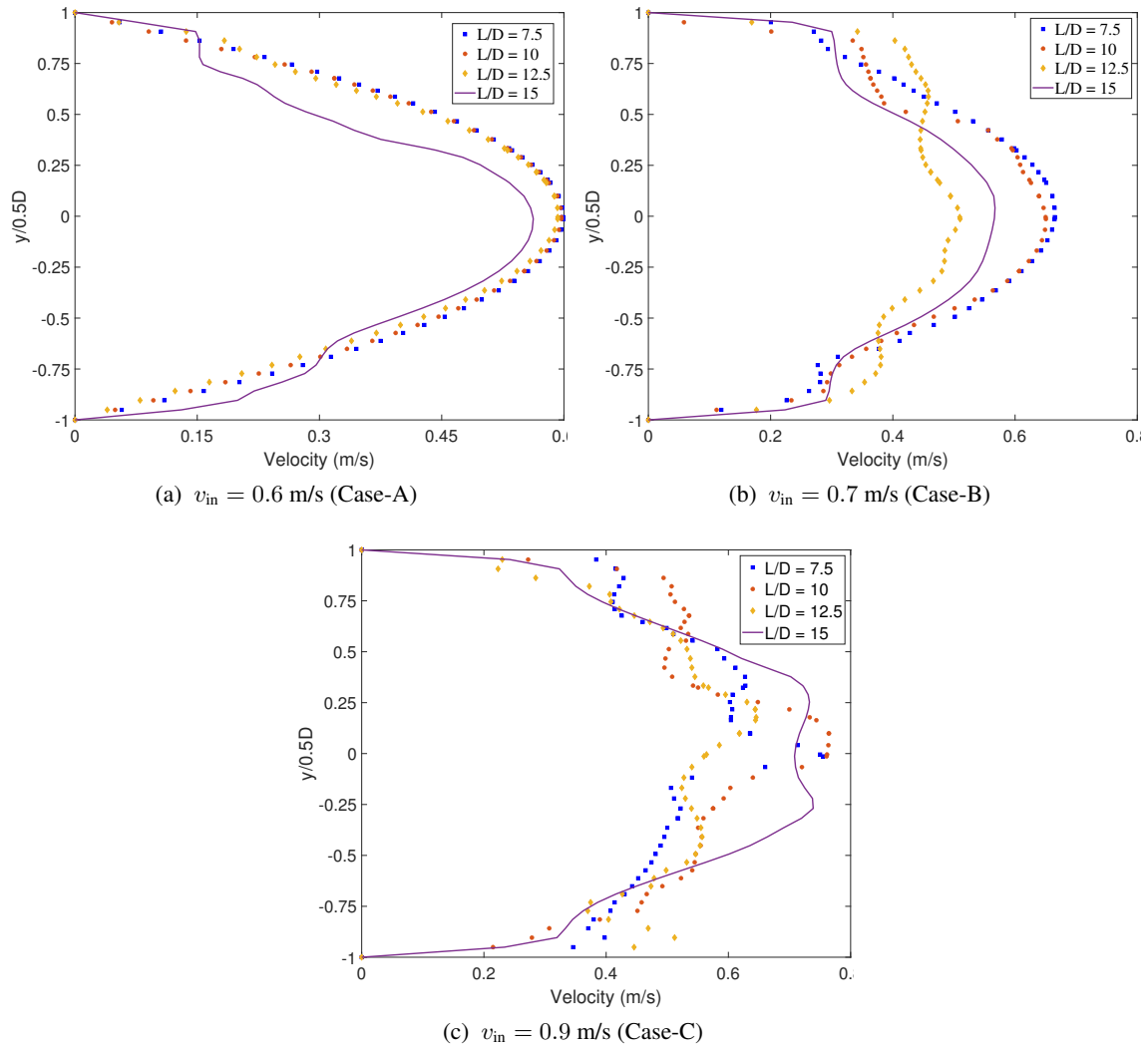


Figure 11: Variation of longitudinal velocity (v_x) across the cross-section of the pipe cut at distances $L = 7.5D$, $10D$, $12.5D$, and $15D$ downstream from the inlet face (refer to cross-sections $P-P$, $Q-Q$, $R-R$, and outlet in Fig.2b) for different inlet velocity conditions

Paul Manneville. Transition to turbulence in wall-bounded flows: Where do we stand? *Mechanical Engineering Reviews*, 2:15–00684, 2016.

Dwight Barkley. Theoretical perspective on the route to turbulence in a pipe. *Journal of Fluid Mechanics*, 803, 2016.

M Eckert. *The Turbulence Problem. A Persistent Riddle in Historical Perspective*. Springer, 2019.

M Eckert. *Turbulence—an Odyssey. Origins and Evolution of a Research Field at the Interface of Science and Engineering*. Springer, 2022.

Mitchell J Feigenbaum. Quantitative universality for a class of nonlinear transformations. *Journal of Statistical Physics*, 19(1):25–52, 1978.

Jerry P Gollub and Harry L Swinney. Onset of turbulence in a rotating fluid. *Physical Review Letters*, 35(14):927, 1975.

Valerii Aleksandrovich Romanov. Stability of plane-parallel couette flow. *Functional Analysis and its Applications*, 7(2):137–146, 1973.

Lev Davidovich Landau and Evgenii Mikhailovich Lifshitz. *Fluid Mechanics*, volume 6. Elsevier, 2013.

Jorge Peixinho and Tom Mullin. Decay of turbulence in pipe flow. *Physical Review Letters*, 96(9):094501, 2006.

- Israel J Wygnanski and FH Champagne. On transition in a pipe. part 1. the origin of puffs and slugs and the flow in a turbulent slug. *Journal of Fluid Mechanics*, 59(2):281–335, 1973.
- Be. A. Toms. Some observations on the flow of linear polymer solutions through straight tubes at large reynolds numbers. *Proceedings of the First International Congress on Rheology*, 2:135–141, 1949.
- AMP Boelens and M Muthukumar. Rotational relaxation time as unifying time scale for polymer and fiber drag reduction. *Physical Review E*, 93(5):052503, 2016.
- H-W Bewersdorff. *Drag Reduction of Turbulent Flows by Additives*. Kluwer, 1995.
- Richard H Nadolink and Wayne W Haigh. Bibliography on skin friction reduction with polymers and other boundary-layer additives. *Applied Mechanics Reviews*, 47:351–460, 1995.
- PK Ptasiniski, BJ Boersma, FTM Nieuwstadt, MA Hulsen, BHAA Van den Brule, and JCR Hunt. Turbulent channel flow near maximum drag reduction: simulations, experiments and mechanisms. *Journal of Fluid Mechanics*, 490: 251–291, 2003.
- Li Xi and Xue Bai. Marginal turbulent state of viscoelastic fluids: A polymer drag reduction perspective. *Physical Review E*, 93(4):043118, 2016.
- John L Lumley. Drag reduction by additives. *Annual Review of Fluid Mechanics*, 1, 1969.
- KY Volokh. An investigation into the stability of a shear thinning fluid. *International Journal of Engineering Science*, 47(5-6):740–743, 2009.
- KY Volokh. Navier-stokes model with viscous strength. *Computer Modeling in Engineering and Sciences*, 92:87–101, 2013.
- KY Volokh. An explanation of the drag reduction via polymer solute. *Acta Mechanica*, 229(10):4295–4301, 2018.
- BV Raghavan and M Ostoja-Starzewski. Shear-thinning of molecular fluids in couette flow. *Physics of Fluids*, 29: 023103, 2017.
- Joseph Smagorinsky. General circulation experiments with the primitive equations: I. the basic experiment. *Monthly Weather Review*, 91(3):99–164, 1963.
- Massimo Germano, Ugo Piomelli, Parviz Moin, and William H Cabot. A dynamic subgrid-scale eddy viscosity model. *Physics of Fluids A: Fluid Dynamics*, 3(7):1760–1765, 1991.
- Franck Nicoud and Frédéric Ducros. Subgrid-scale stress modelling based on the square of the velocity gradient tensor. *Flow, Turbulence and Combustion*, 62(3):183–200, 1999.
- Douglas K Lilly. A proposed modification of the germano subgrid-scale closure method. *Physics of Fluids A: Fluid Dynamics*, 4(3):633–635, 1992.
- Mikhail L Shur, Philippe R Spalart, Mikhail Kh Strelets, and Andrey K Travin. A hybrid rans-les approach with delayed-des and wall-modelled les capabilities. *International Journal of Heat and Fluid Flow*, 29(6):1638–1649, 2008.